Supporting information

Robust oxygen electrocatalysis enabled by bulk nitrogen-doped hierarchical structure cobalt carbide

Caimei He, Danling Zhang, Yezheng Cai*, Cheng Hou*, Xiangsi Wu, Zhaoling Ma, Youguo Huang, Hongqiang Wang, Qingyu Li*

Guangxi Key Laboratory of Low Carbon Energy Materials, Guangxi New Energy Ship Battery Engineering Technology Research Center, Guangxi scientific and technological achievements transformation pilot research base of electrochemical energy materials and devices, School of Chemistry and Pharmaceutical Sciences, Guangxi Normal University, Guilin 541004, China

*Corresponding authors:

yezhengcai@163.com (Y. Cai);

houcheng@gxnu.edu.cn (C. Hou);

liqingyu62@126.com (Q. Li).

1 Experimental parts

1.1 Materials

Electronically conductive carbon black (EC, ECP600JD) was purchased from Lion Corporation. $Co(NO_3)_2 \cdot 6H_2O$, urea, zinc acetate ($Zn(Ac)_2$), potassium hydroxide (KOH), and Melamine (M) were provided by Sinopharm Chemical ReagentCo., Ltd. Commercial Pt/C and RuO_2 catalysts were purchased from Aladdin.

1.2 Synthesis of EC coupled with CoO nanoparticles-based hierarchical structure (CoO NPHS/EC)

CoO NPHS was synthesized via a hydrothermal process and followed by heat treatment. Specifically, 200 mg urea, 1200 mg $Co(NO_3)_2 \cdot 6H_2O$, and 70 mg activated carbon black were dispersed in 50 mL deionized water and put into the Teflon-lined autoclave, which was then heated to 160 °C for 10 h. After cooling down, the obtained hydrothermal Co precursor was centrifuged, washed with deionized water, and dried at 80 °C for 10 h. The dried Co precursor was then heated to 350 °C under N_2 gas flow and kept at this temperature for 2 h. After cooling down to room temperature, CoO NPHS was obtained.

1.3 Synthesis of EC coupled with nitrogen doped Co carbide hierarchical structure (N-Co_2C HS/EC)

Melamine and CoO NPHS/EC with a mass ratio of 50:1 were spread in two porcelain boats with the former located upstream in the tube furnace. These samples were then heated to 500 °C with a heating rate of 5 °C/min. After heat treatment for 1 h, the obtained catalyst was naturally cooled down to room temperature and was

marked as N-Co_2C HS/EC.

1.4 Synthesis of N-Co-CoO HS/EC, N-CoO-Co_2C HS/EC, and N-Co HS/EC.

N-Co-CoO HS/EC, N-CoO-Co_2C HS/EC, and N-Co HS/EC were prepared via a process similar to that of N-Co_2C HS/EC by simply controlling the melamine : CoO NPHS/EC mass ratio as 10:1, 30:1, and 100:1, respectively.

1.5 Structural characterizations

The crystal structure features of the catalysts were confirmed by X-ray diffraction (XRD, Rigaku D/max 2500). The lattice expansion of N-Co_2C HS/EC was calculated according to the equation of $\Delta a = \frac{a_{catalyst} - a_0}{a_0}$, where Δa was the lattice expansion, $a_{catalyst}$ and a_0 were the lattice parameters of measured catalyst and pure Co_2C, respectively. The lattice parameter of a catalyst was calculated based on the (111) diffraction peak position. The micro structure features were characterized by Helios NanoLab 600i scanning electron microscopy (SEM), JEM-2100f transmission electron microscopy (TEM), and high-resolution transmission electron microscopy (HRTEM). The surface compositions and chemical features were examined by Thermo Scientific K-Alpha+ X-ray photoelectron spectroscopy (XPS). Jobin Ybon, T6400 Raman spectrometer was used to record the Raman spectrum. Soft X-ray absorption near-edge structure (XANES) tests were used to reveal the chemical configurations.

1.6 Electrochemical performance evaluations

The ORR and OER catalytic performance of all the prepared catalysts was evaluated in a standard three-electrode system connected with a CHI760E

electrochemical workstation at room temperature. The reference and counter electrodes were Ag/AgCl electrode (saturated KCl) and graphite rod, respectively. The working electrode was prepared by coating an appropriate catalyst on the polished glassy carbon electrode with a geometric area of 0.196 cm^2. Specifically, 5 mg catalyst was dispersed in the solution composed of 990 μL absolute ethanol and 10 μL of Nafion (5 wt.%) by ultrasonic treatment, forming a catalyst dispersion ink with a mass concentration of 5 mg mL^{-1}. Then, 20 μL of catalyst dispersion ink was coated on the glassy carbon electrode and dried in the air naturally; the catalyst loading of catalyst on GCE is 0.51 mg cm^{-2}. For commercial Pt/C catalyst, 1 mg/mL ink was prepared by the same process above. Then, 20 μL Pt/C ink was coated on the glassy carbon electrode and dried in the air naturally, and the loading is 0.10 mg cm^{-2}. For metal-air battery performance evaluation, Pt/C + RuO_2 ink (1 mg mL^{-1}) was prepared similar to Pt/C ink with a Pt/C:RuO_2 mass ratio of 1:1.

For ORR, the cyclic voltammetry (CV) and linear sweep voltammetry (LSV) curves were recorded in O_2-saturated 0.1 M KOH aqueous solution. The CV curves were recorded at a scan rate of 200 mV s^{-1}, and the LSV curves were recorded at scan rate of 5 mV s^{-1} and a rotation speed of 1600 rpm. All the present potentials in this work were corrected to the hydrogen standard electrode (RHE) potential according to the equation of $E_{RHE} = E_{Ag/AgCl} + 0.197 + 0.059*pH$. The kinetic current density (j_k) of the catalyst was calculated based on the follow equation (1).

$$1/j = 1/j_L + j_K \quad (1)$$

where j was the measured current density and j_L was the limiting current.

The catalytic mechanism was further examined by carrying out a rotating ring disk electrode (RRDE) measurement. The hydrogen peroxide H_2O_2 *yield* and electron transfer number (n) were calculated according to the (2) and (3) equations[1].

$$H_2O_2\ (\%)=200I_r/(I_r + N*I_d) \quad (2)$$

$$n=4NI_d/(I_r + N*I_d) \quad (3)$$

where I_r, I_d, and N are the disk current, ring current, and collection efficiency (0.37), respectively. The electrochemically active surface area (ECSA) of the catalyst was evaluated by the CV method to calculate the double layer capacitance, which was proportional to ECSA.

For OER, the LSV curves were recorded in 1 M and/or 0.1 M KOH aqueous solution at a scan rate of 5 mV s^{-1} with current drop compensation. The working electrode was made by coating 20 μL catalyst ink on the carbon paper with an area of 0.5*1 cm^2 and dried in air.

1.7 Zinc-air battery performance

A homemade ZAB was assembled by using polished Zn foil, carbon paper coated by prepared catalyst with an area loading of 2 mg cm^{-2}, 6 M KOH + 0.2 M $Zn(Ac)_2$ aqueous solution as anode, cathode, and electrolyte, respectively. The discharging and charging polarization curves were recorded at a scan rate of 10 mV s^{-1}. The discharging specific capacity curves were recorded at a current density of 10 mA cm^{-2}. The discharging/charging cycling curves were recorded at 20 mA cm^{-2} with 10 min for each cycle.

1.8 Density functional theory (DFT) calculations

The free energies calculations were performed by using MedeA-VASP[2], taking advantage of the density functional theory (DFT) and the Projected Augmented Wave (PAW) method. For the exchange–correlation functional, we adopted the generalized gradient approximation (GGA) in the form of the Perdew– Burke–Ernzerhof (PBE) formulism.[3] For all the geometry optimizations, the cutoff energy was set to be 500 eV. In order to eliminate the interaction between adjacent substrates, a vacuum region of 20Å is set in the Z-axis. The k-point mesh of 2×2×1 Γ-centered grids in the first Brillouin zone was sampled for the energy and electronic structure calculations. The convergence criteria of energy and force were set to 1×10^{-6} eV and 0.01 eVÅ^{-1}, respectively. All atoms were fully relaxed in the process of structural optimization and have been confirmed to be the minimum with no imaginary frequencies.

the ORR process goes through a 4e transfer mechanism in an alkaline environment that is described by the following equations:

$$* + O_2 + H_2O + e^- \rightarrow *OOH + OH^- \quad (4)$$

$$*OOH + e^- \rightarrow *O + OH^- \quad (5)$$

$$*O + H_2O + e^- \rightarrow *OH + OH^- \quad (6)$$

$$*OH + e^- \rightarrow * + OH^- \quad (7)$$

Here,*denotes active sites on the catalyst surface,and OH*, O*, and OOH* denotes the corresponding adsorbed intermediates.

We can obtain the Gibbs free energy of each elementary step by using the computational hydrogen electrode (CHE) model proposed by Nørskov et al.[4] According to this model, the change in the Gibbs free energy (ΔG) of each reaction was calculated as follow:

$$\Delta G = \Delta E + \Delta E_{ZPE} - T\Delta S + \Delta G_{pH} + eU \quad (8)$$

Among them, ΔE is the adsorption energy of each reaction intermediate which can be calculated by DFT. ΔE_{ZPE} is the change of the zero-point energy and ΔS is the entropy change before and after the reaction (T=298.15 K). ΔG_{PH} is the free energy

correction with respect to the H concentration in solution, e.g., $\Delta G_{PH} = k_B T \ln 10 \times pH$, where k_B is Boltzmann's constant. In this work, the value of the pH was set to 13 to simulate a strong alkaline environment e and U are the number of transferred electrons and the applied electrode potential, respectively. Then, at standard conditions, the free energy change for all ORR electrochemical steps ($\Delta G_{1\text{-}4}$) can be expressed as:

$$\Delta G_1 = 1.84 - \Delta G_{*OOH} \quad (9)$$

$$\Delta G_2 = \Delta G_{*OOH} - \Delta G_{*O} \quad (10)$$

$$\Delta G_3 = \Delta G_{*O} - \Delta G_{*OH} \quad (11)$$

$$\Delta G_4 = \Delta G_{*OH} \quad (12)$$

It should be noted that we investigated the electrochemical processes employing the established computational hydrogen electrode (CHE) model. The theoretical basis for the validity of the CHE model is that electrochemical reactions that happened in the solution normally possess small kinetic barriers, which are surmountable at room temperature. The reaction kinetics will thus be dictated by merely the free energy difference of each step. The step with the most positive free energy difference is therefore the rate-determining step. Therefore, the theoretical overpotential η is defined in equation (S10):

$$\eta_{Theory} = 0.46\ V - \min\{\Delta G_1, \Delta G_2, \Delta G_3, \Delta G_4\}/e \quad (13)$$

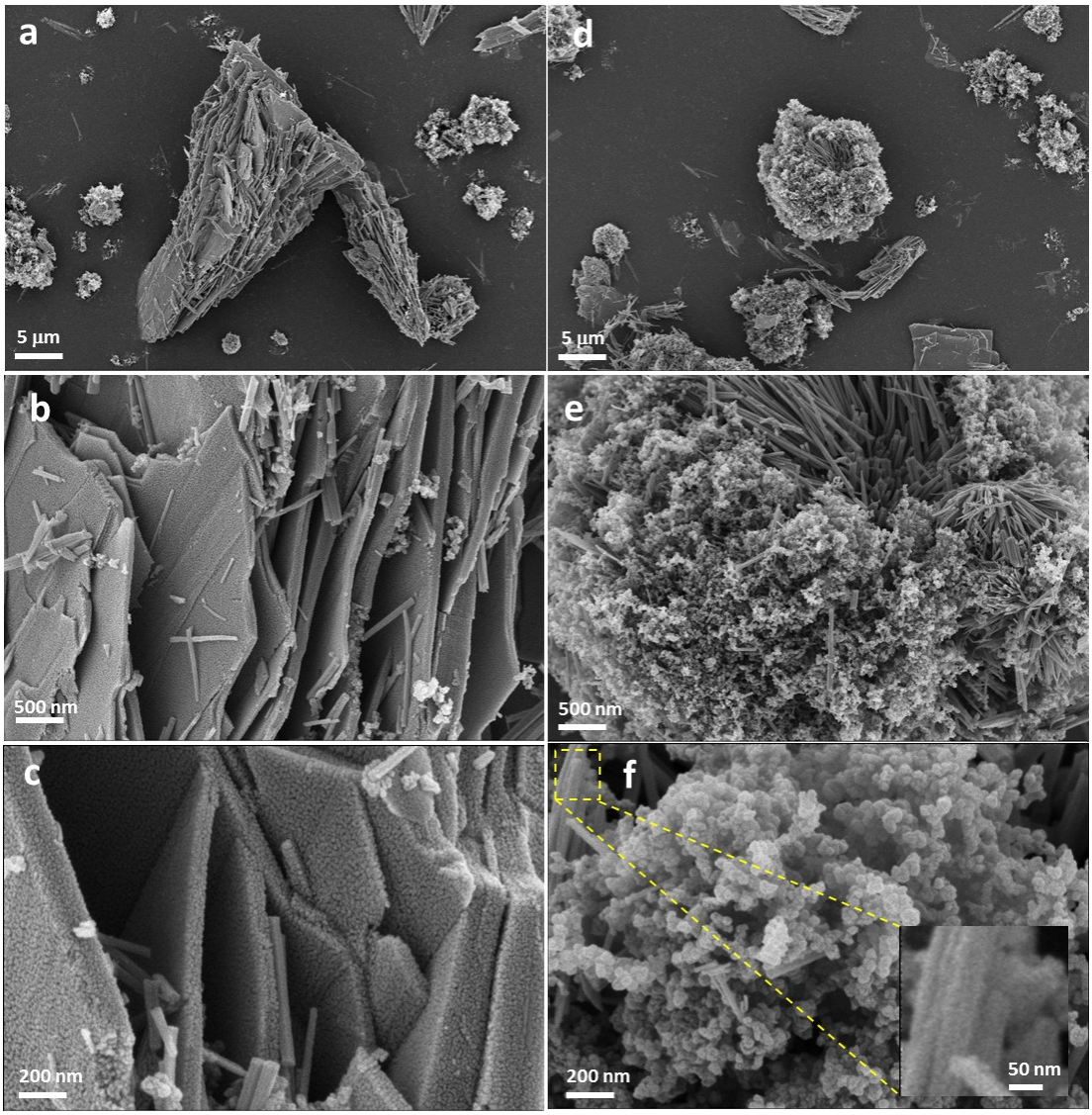

Fig. S1 (a-c) SEM images at magnifications of CoO NPHS/EC show the nano sheets feature; (d-f) SEM images at magnifications of CoO NPHS/EC show the nano rods feature.

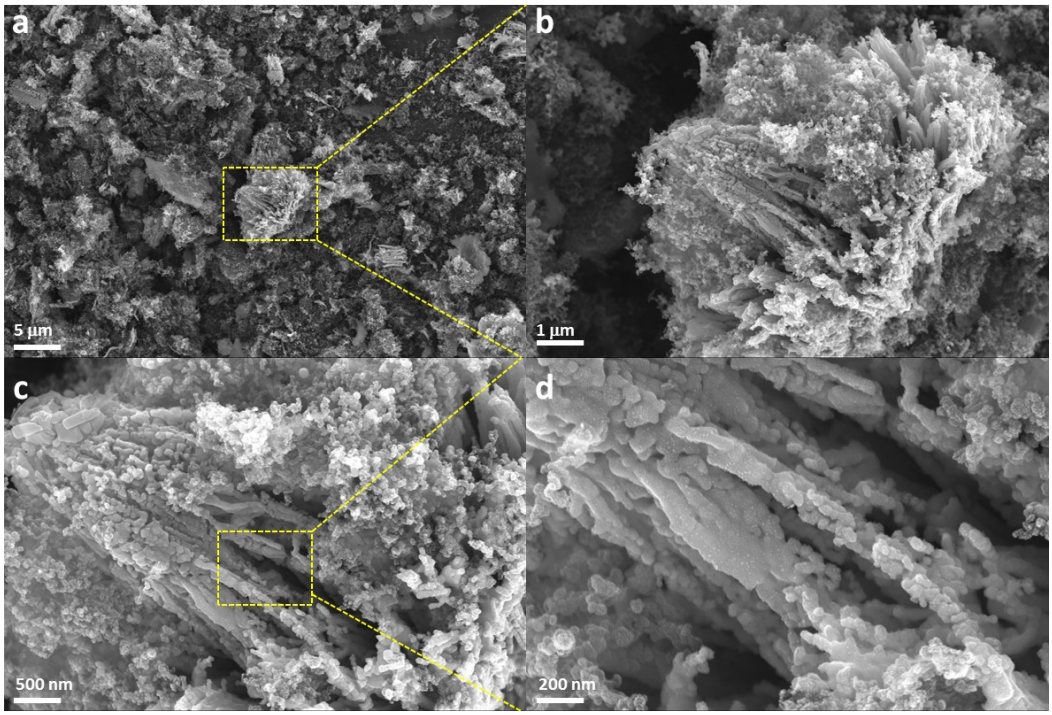

Fig. S2 SEM images of N-Co_2C HS/EC at different magnifications.

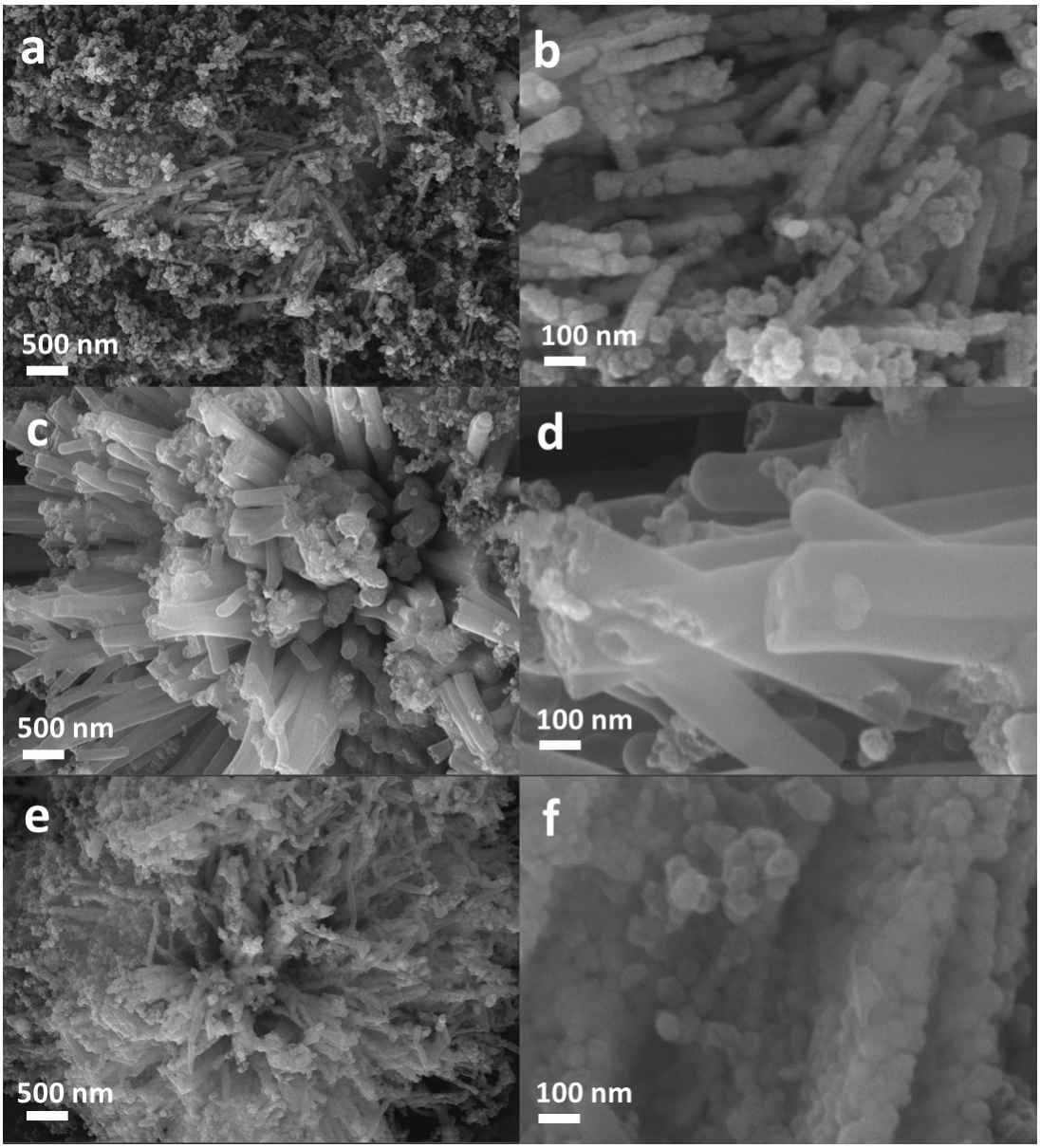

Fig. S3 SEM images of (a, b) N-Co-CoO HS/EC, (c and d) N-CoO-Co_2C HS/EC, and (e and f) N-Co HS/EC.

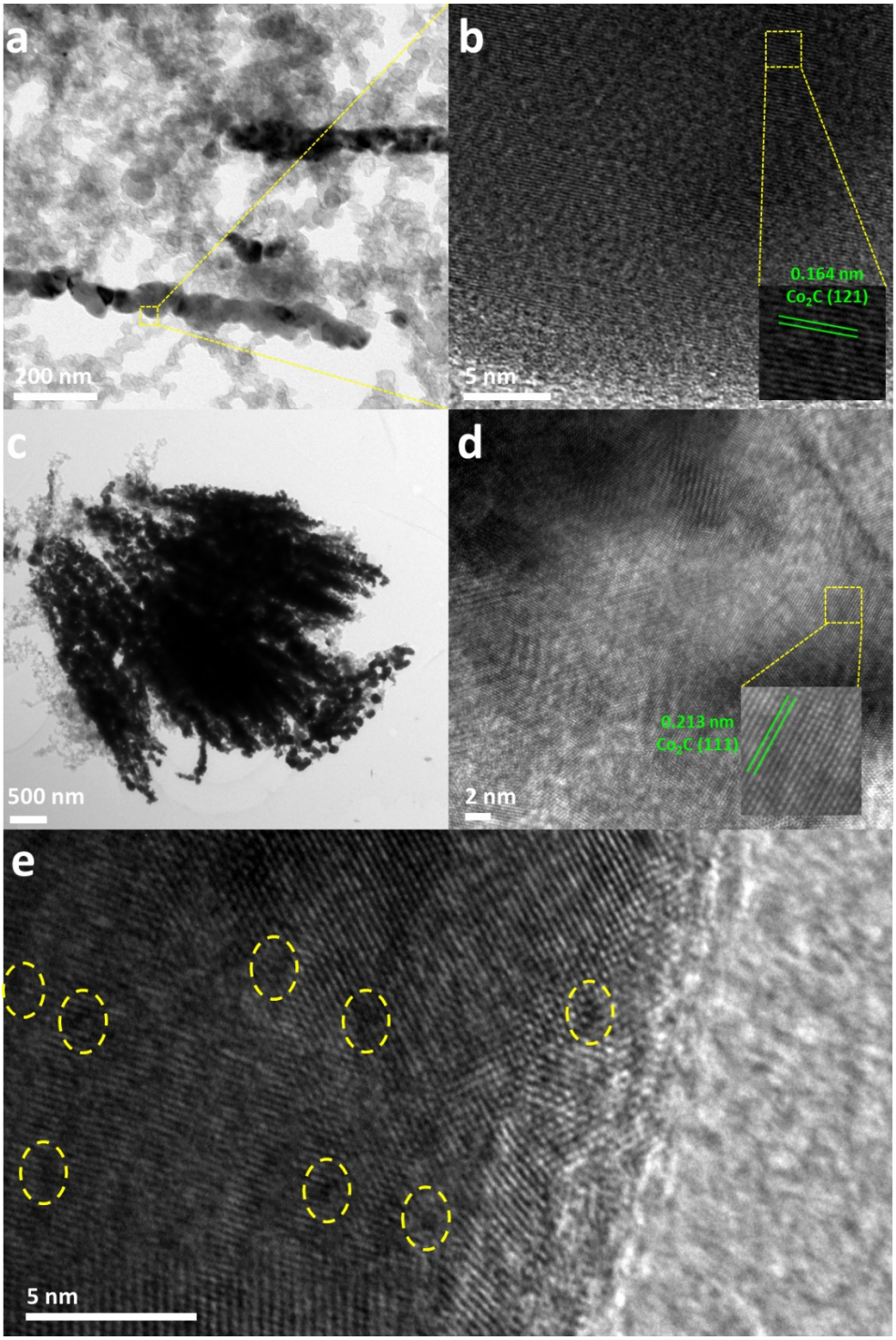

Fig. S4 (a)TEM and (b) HRTEM images of N-Co_2C HS/EC.

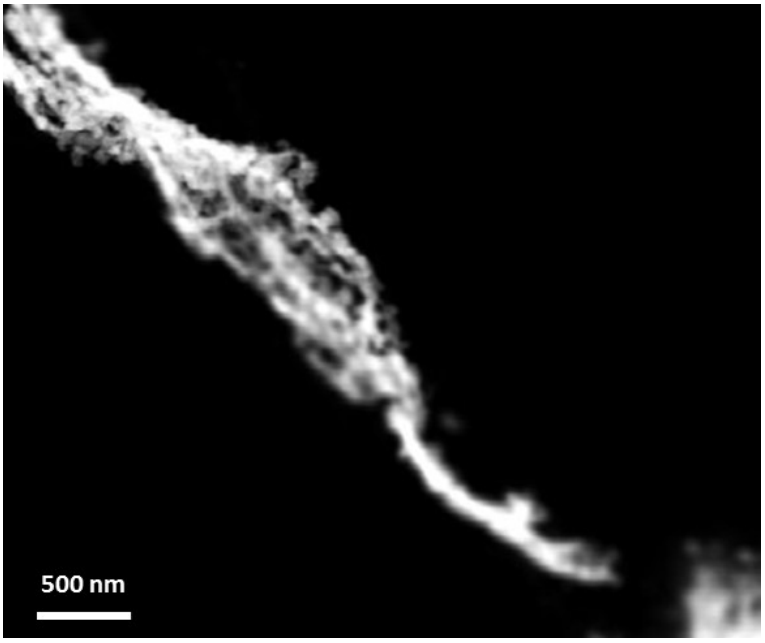

Fig. S5 HAADF-STEM image of N-Co_2C HS/EC.

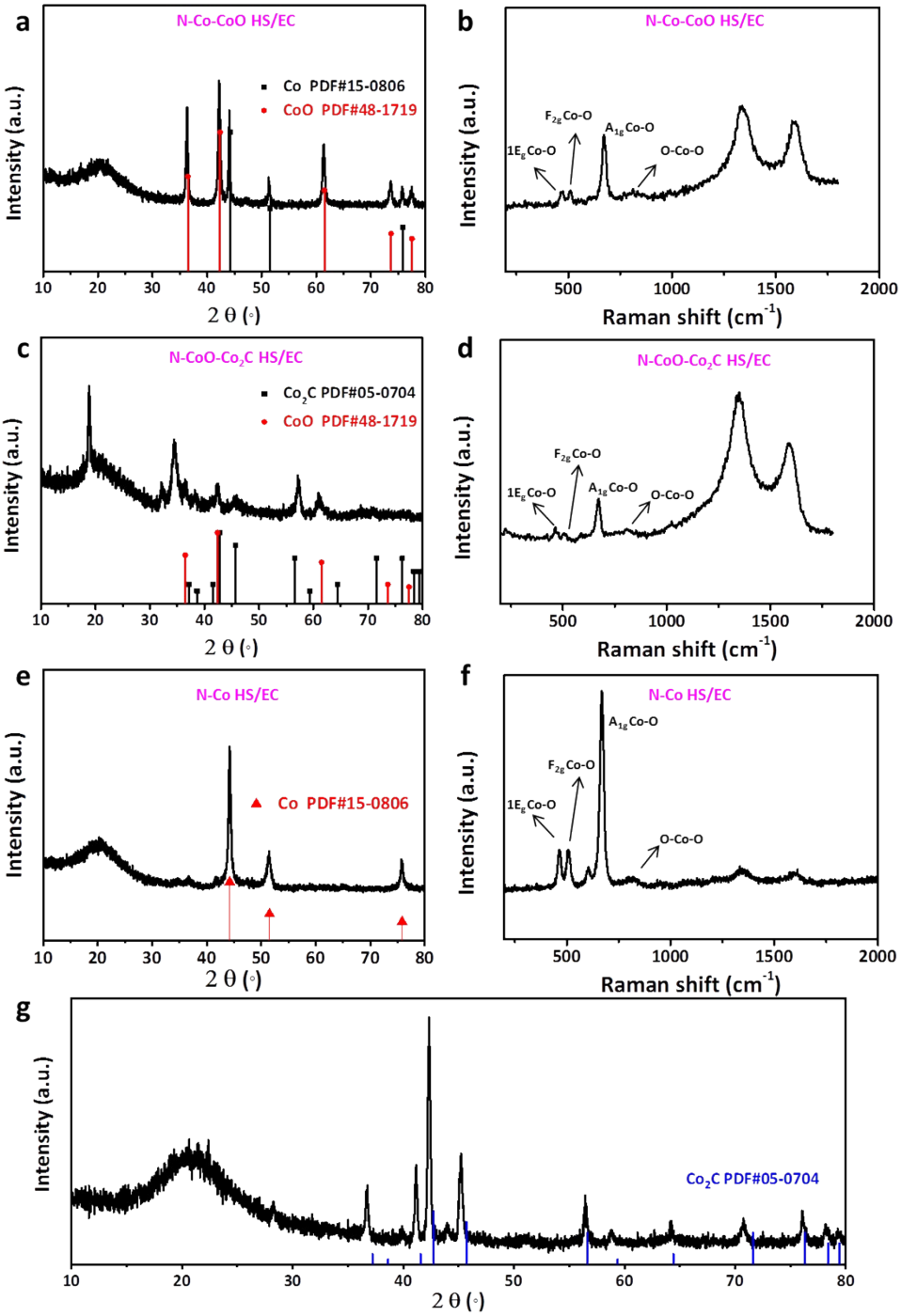

Fig. S6 XRD patterns and ex-situ Raman spectrum of (a and b) N-Co-CoO HS/EC, (c and d) N-CoO-Co_2C HS/EC, and (e and f) N-Co HS/EC; (g) XRD pattern of N-Co_2C HS.

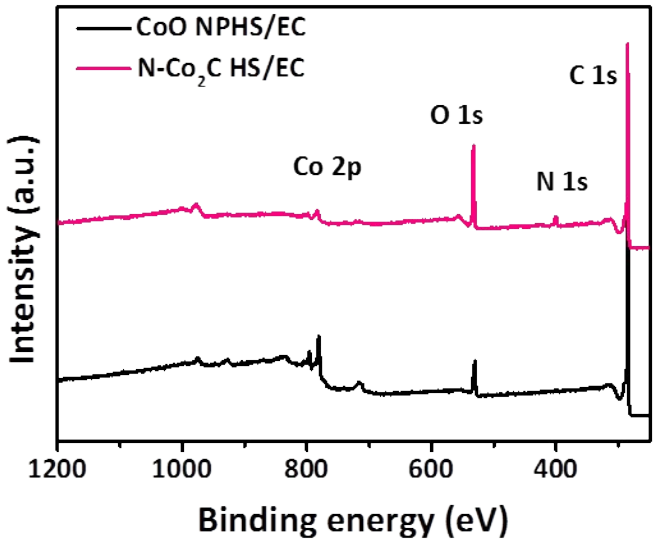

Fig. S7 XPS survey of CoO NPHS/EC and N-Co_2C HS/EC.

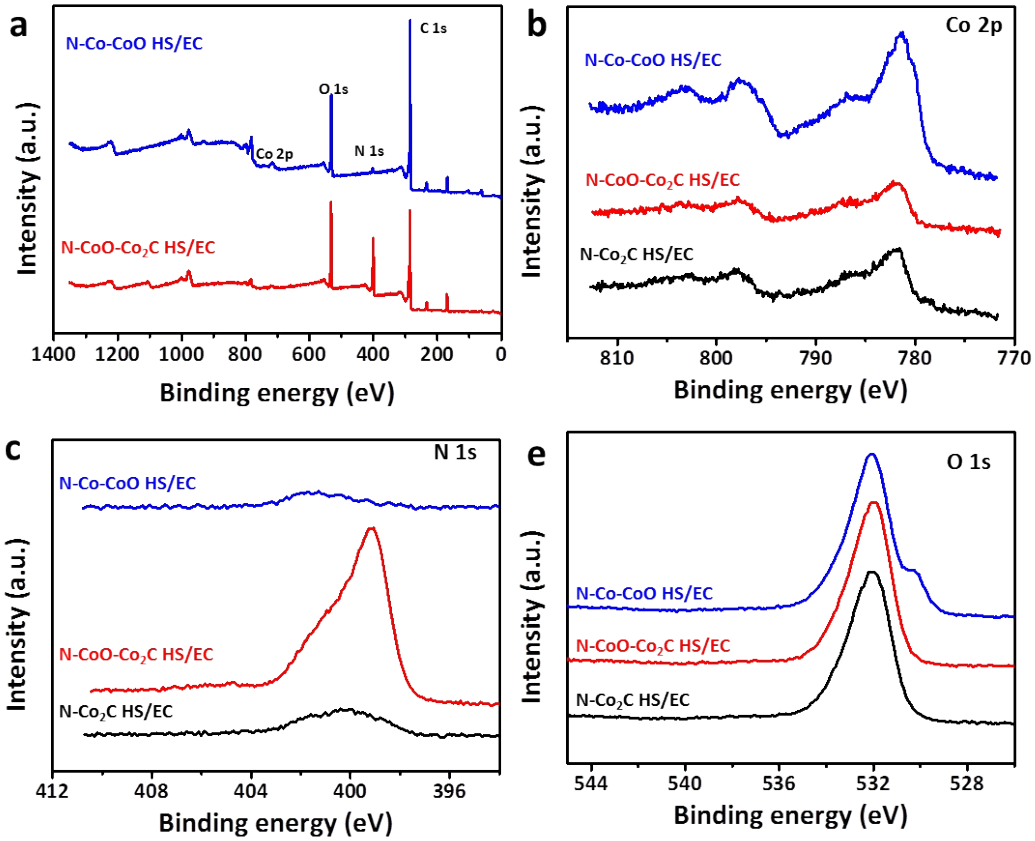

Fig. S8 (a) XPS survey of N-Co-CoO HS/EC and N-CoO-Co_2C HS/EC; (b-d) High resolution Co 2p, N 1s, and O 1s spectrum of N-Co-CoO HS/EC, N-CoO-Co_2C HS/EC, and N-Co_2C HS/EC.

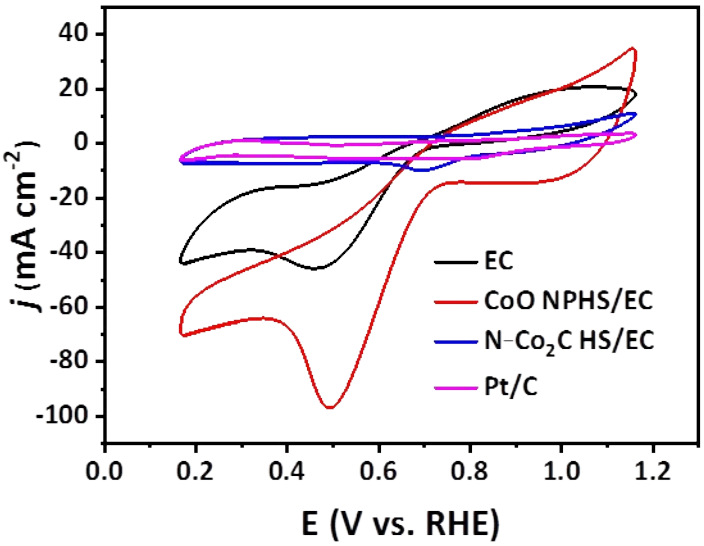

Fig. S9 CV curves of EC, CoO NPHS/EC, N-Co_2C HS/EC, and Pt/C in O_2-saturated 0.1 M KOH aqueous solution.

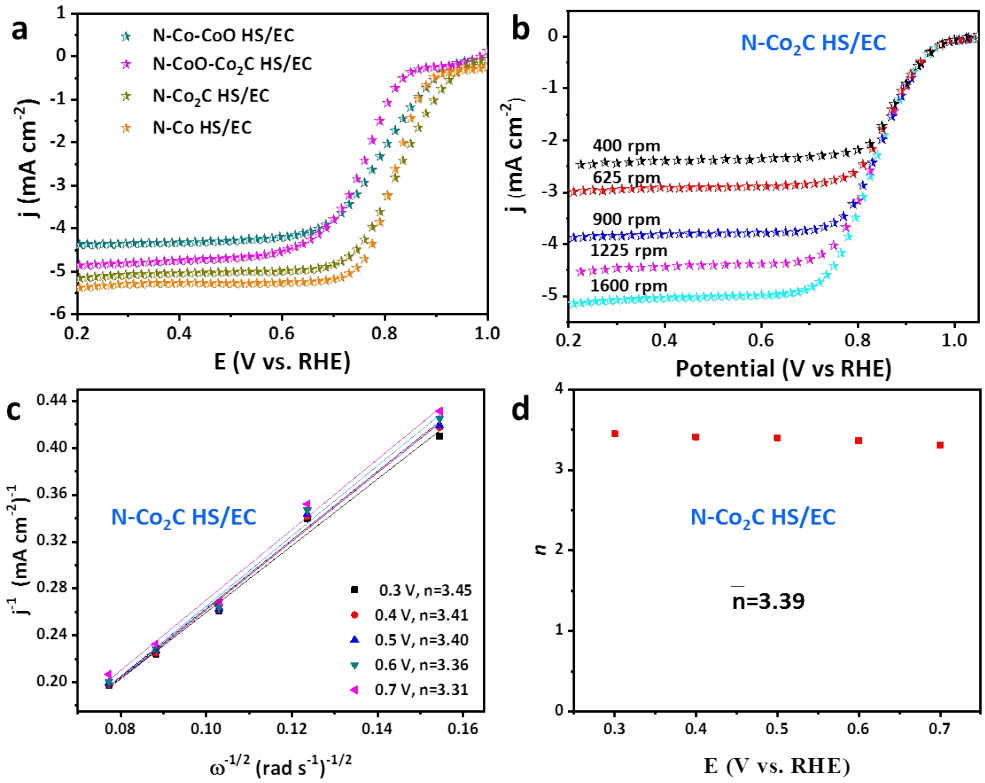

Fig. S10 (a) LSV curves of N-Co-CoO HS/EC, N-CoO-Co_2C HS/EC, N-Co_2C HS/EC, and N-Co HS/EC; (b-d) LSV curves at different rotation speeds (b), K-L plots (c), and electron transfer number (n) (d) of N-Co_2C HS/EC.

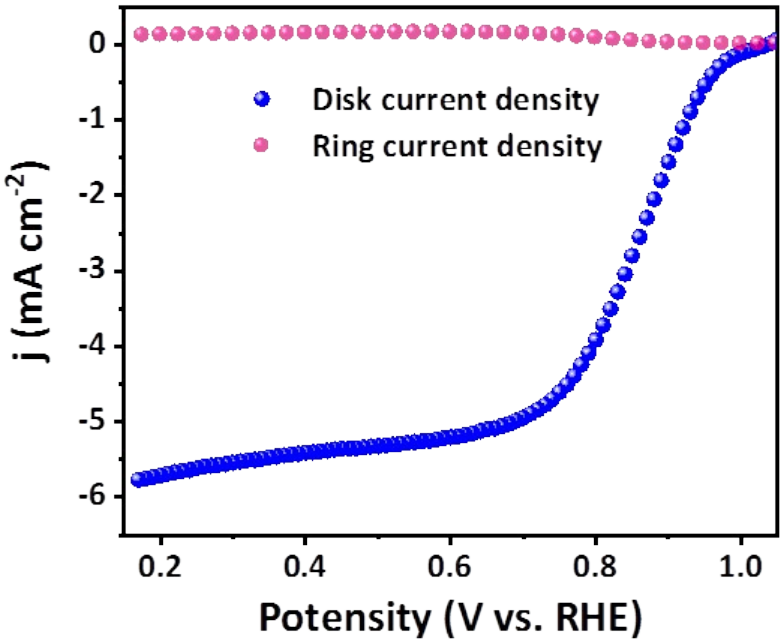

Fig. S11 RRDE curve of N-Co_2C HS/EC.

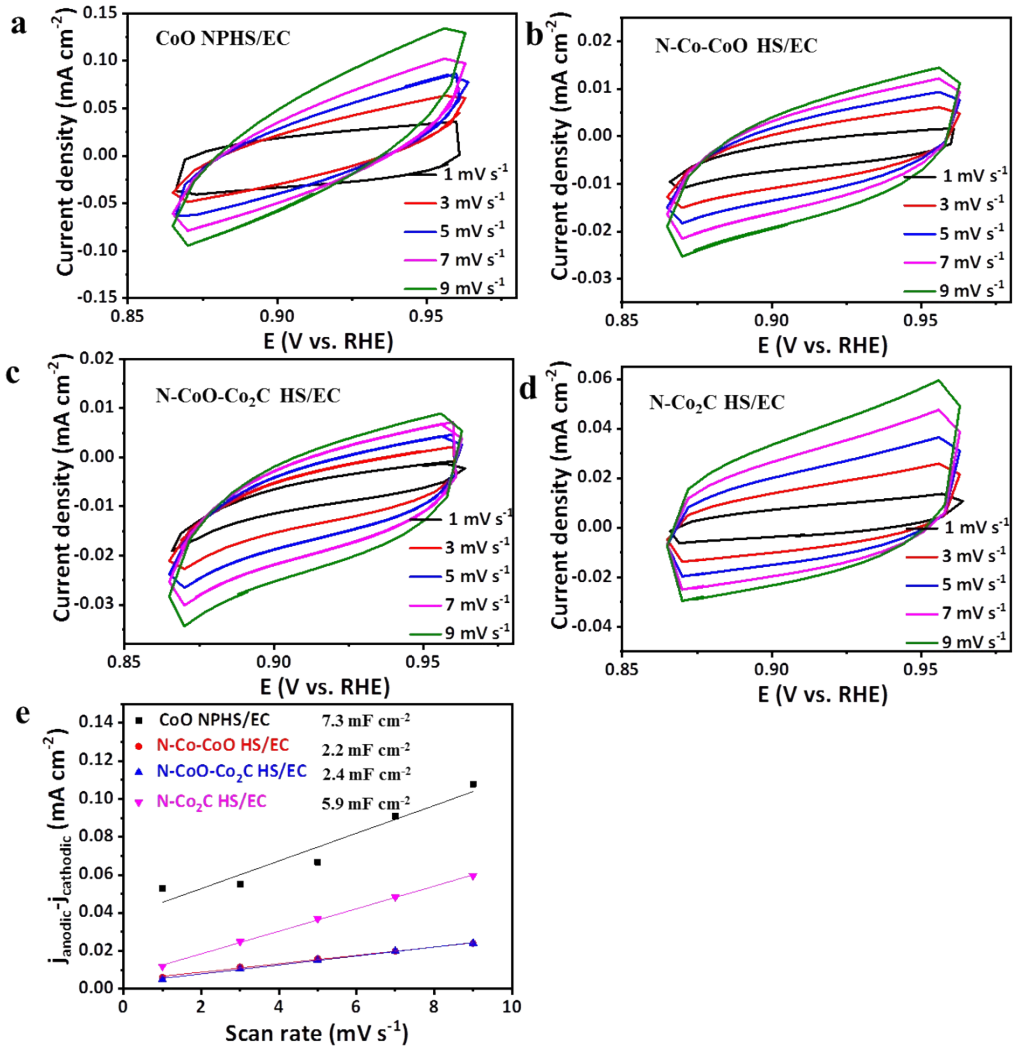

Fig. S12 (a-d) CV curves and the current density difference ($\Delta j=j_a-j_c$) at 0.73 V plotted against scan rate of the catalysts; (e) The difference in anodic and cathodic current density ($\Delta j=j_{anodic}-j_{cathodic}$) plotted against scan rate of the as-prepared catalysts.

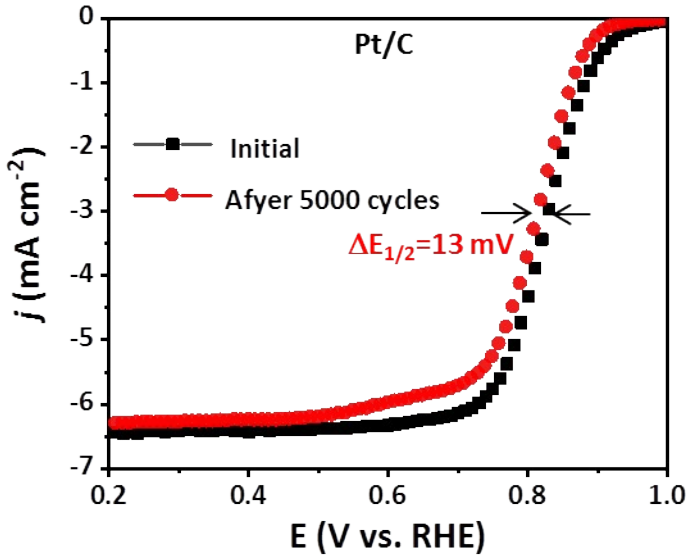

Fig. S13 LSV curves of Pt/C before and after 5000 CV scans.

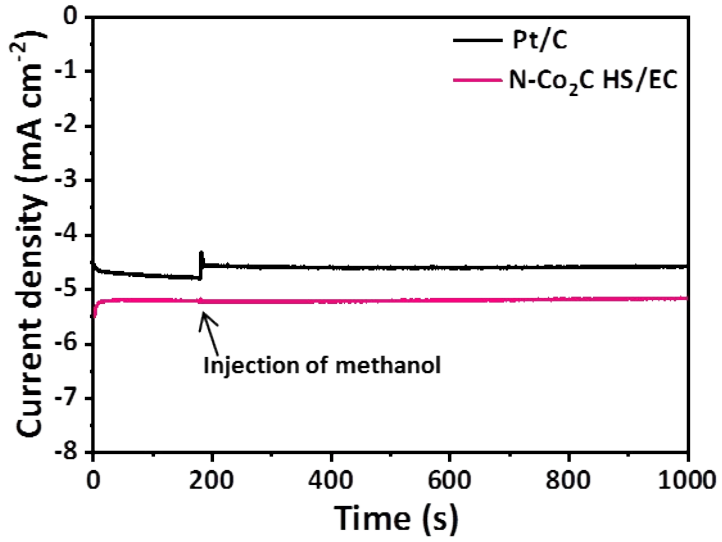

Fig. S14 Chronoamperometric i-t curves of Pt/C and N-Co_2C HS/EC with the addition of 2 mL methanol in 0.1 M KOH.

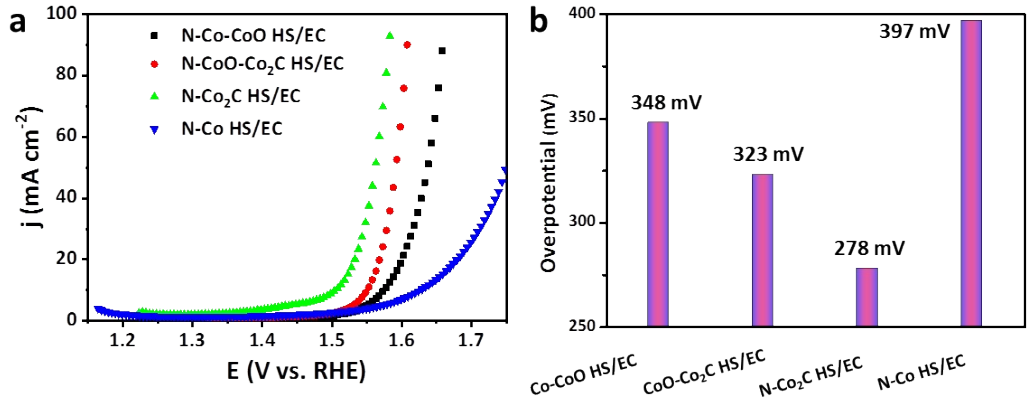

Fig. S15 (a) OER LSV curves and (b) the overpotential values at 10 mA cm^{-2} of N-Co-CoO HS/EC, N-CoO-Co_2C HS/EC, N-Co_2C HS/EC, and N-Co HS/EC.

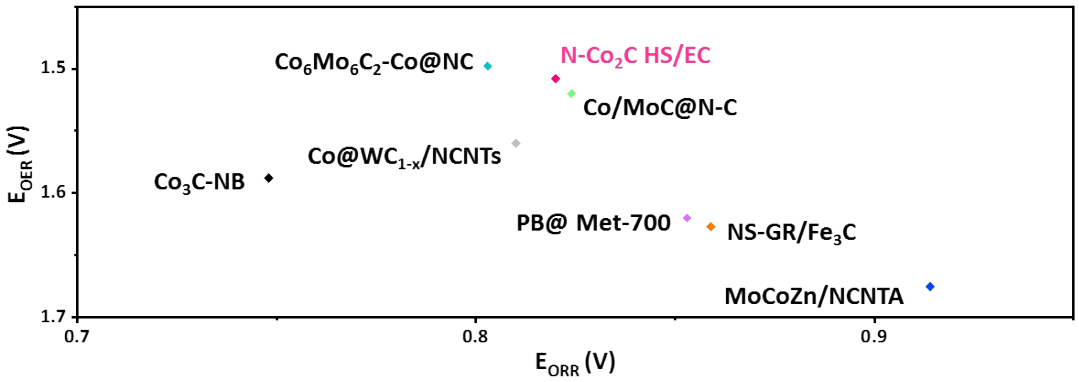

Fig. S16 Diagram of bifunctional ORR and OER activities of N-Co_2C HS/EC and reported bifunctional carbide catalysts in 0.1 M KOH aqueous solution.

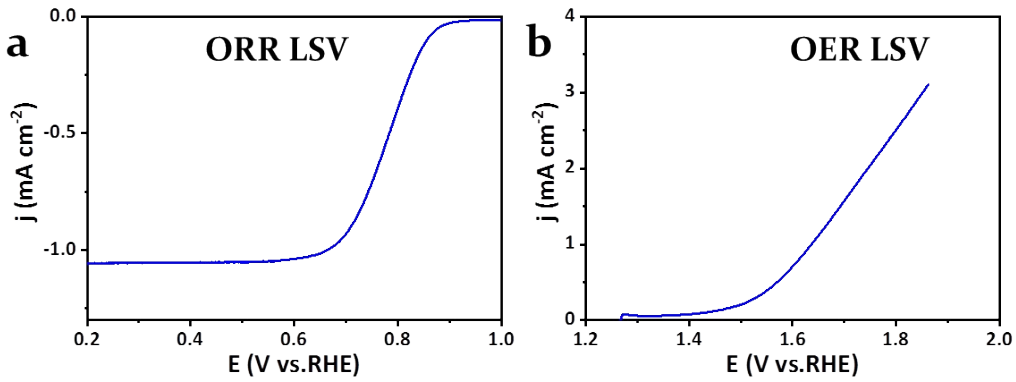

Fig. S17 In situ LSV curve of of N-Co_2C HS in 1.0 M KOH for (a) ORR and (b) OER at different potentials at a scanning rate of 0.3 mV s^{-1}.

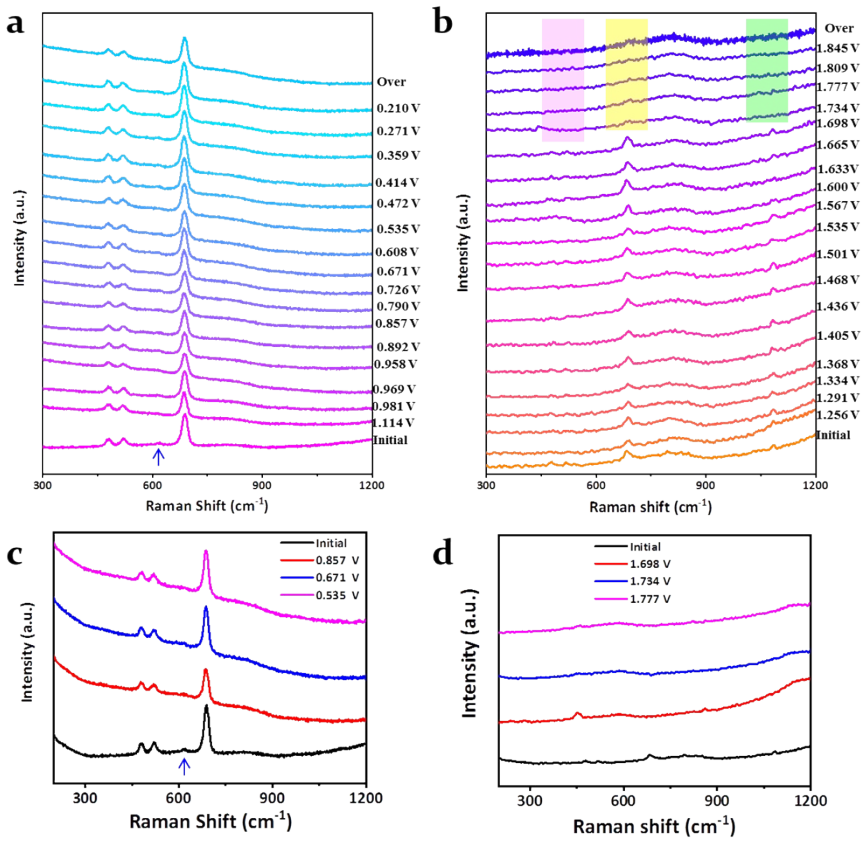

Fig. S18. In situ Raman spectrum of N-Co_2C HS/EC in 1.0 M KOH for (a,c) ORR and (b,d) OER at different potentials.

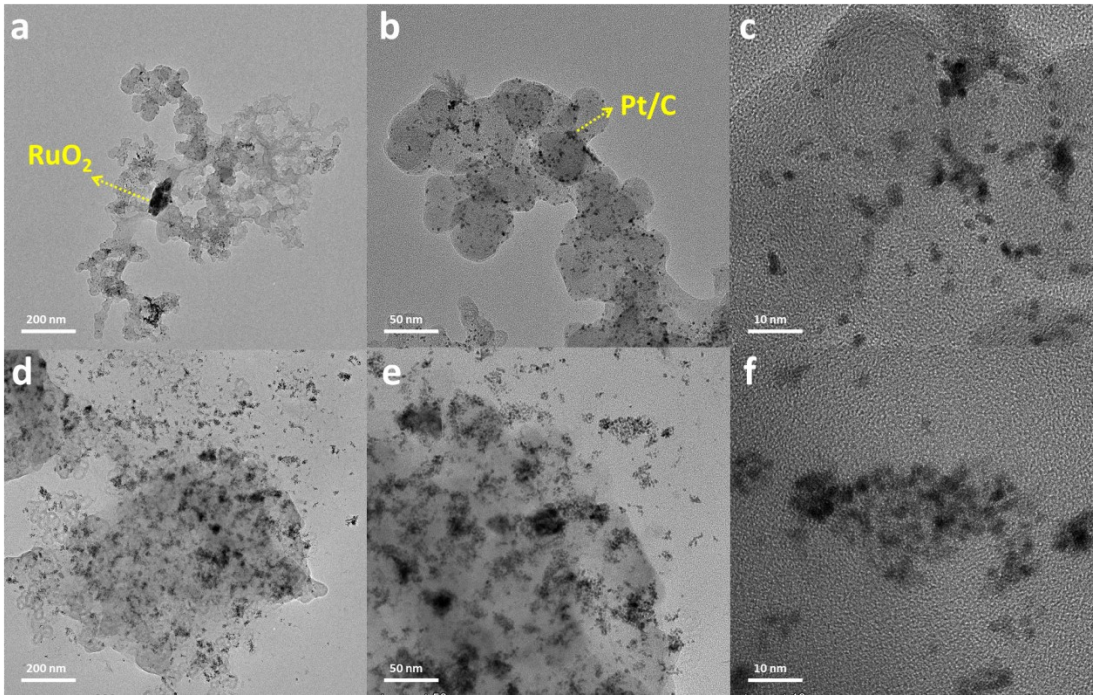

Fig. S19 TEM images of Pt/C + RuO_2 mixed catalysts (a-c) before and (d-f) after charging and discharging in ZAB for 37 h.

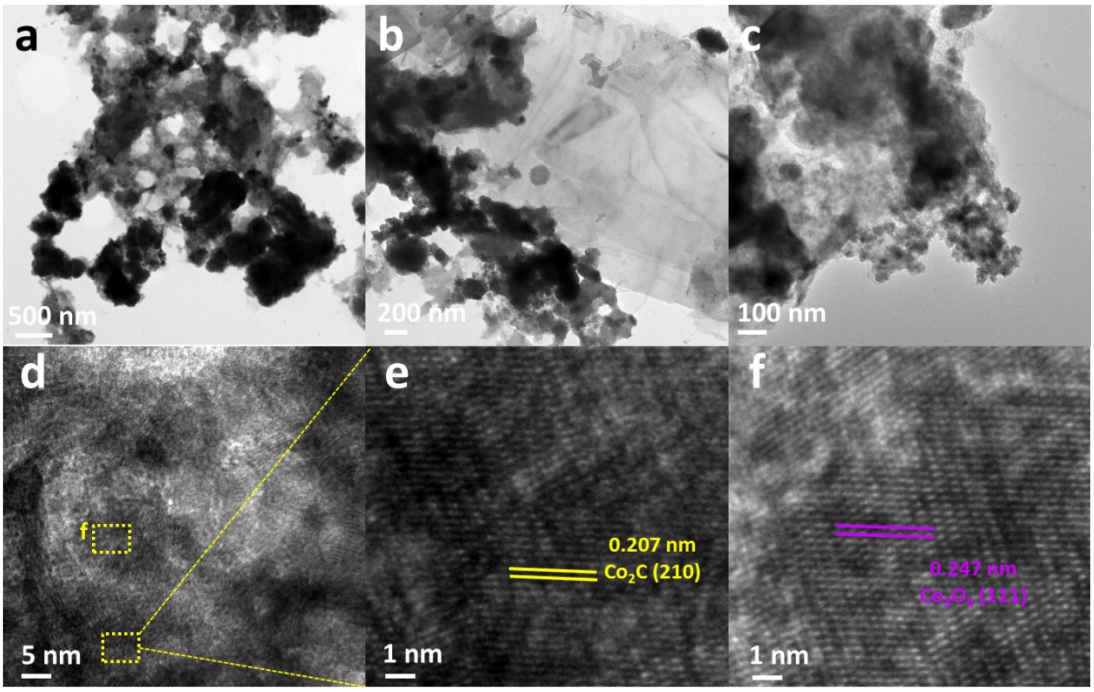

Fig. S20 TEM images of N-Co_2C HS/EC catalyst after charging and discharging in ZAB for 47 h.

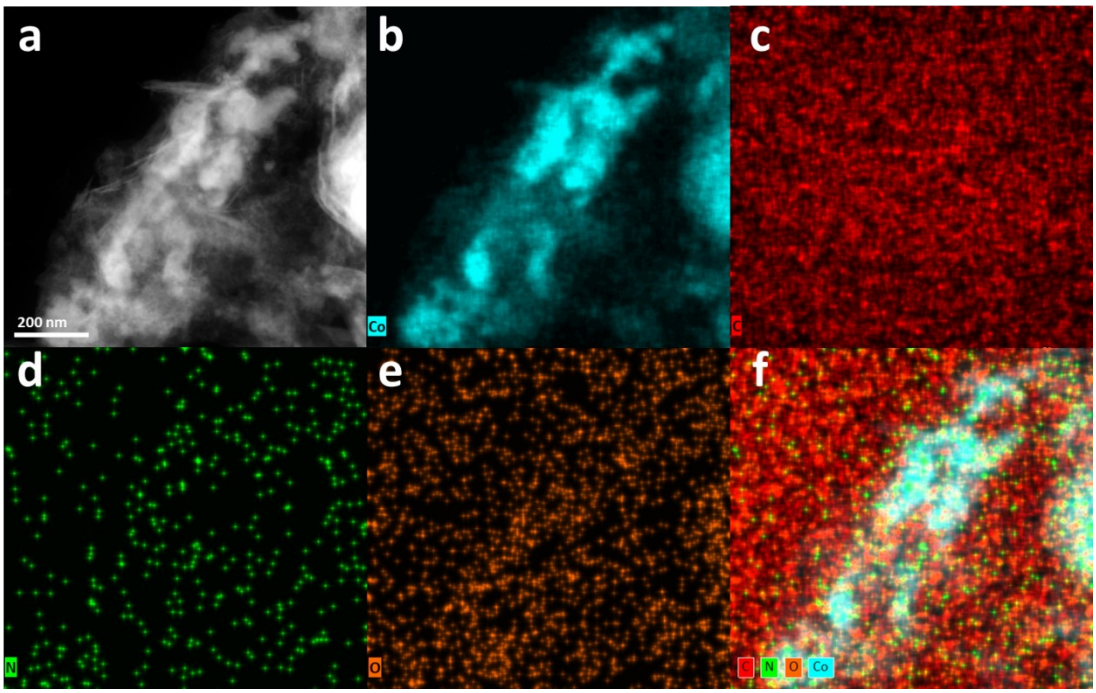

Fig. S21 TEM image and the elemental mappings of N-Co_2C HS/EC catalyst after charging and discharging in ZAB for 47 h.

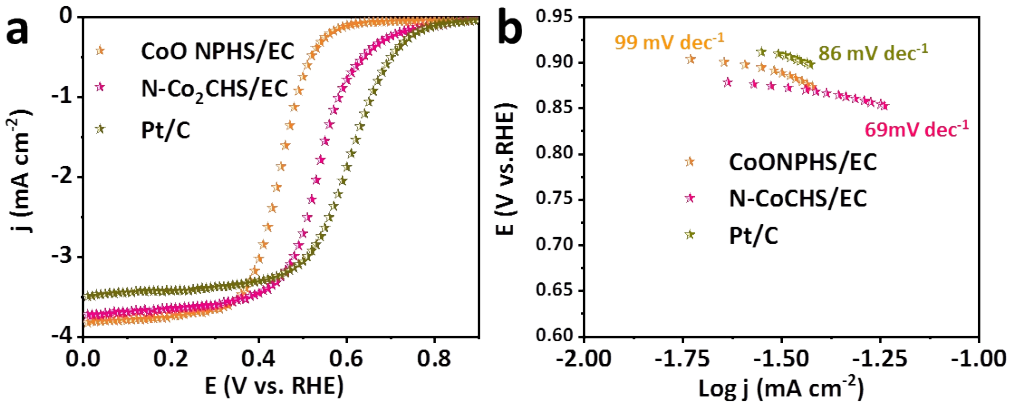

Fig. S22 (a) ORR LSV curves and (b) Tafel plots of CoO NPHS/EC, N-Co_2C HS/EC, and Pt/C in 1 M NaCl electrolyte.

Table S1 Surface compositions of CoO NPHS/EC, N-Co-CoO HS/EC, N-CoO-Co_2C HS/EC, and N-Co_2C HS/EC examined by XPS.

Catalyst	**Atomic ratio (%)**			
	Co	**N**	**C**	**O**
CoO NPHS/EC	4.56	0.87	85.55	9.02
N-Co-CoO HS/EC	3.24	3.38	74.27	19.12
N-CoO-Co_2C HS/EC	1.34	22.74	57.55	18.37
N-Co_2C HS/EC	1.51	4.72	78.15	15.62

Table S2 $E_{1/2}$ values of N-Co_2C HS/EC and the reported carbide catalysts for ORR in 0.1 M KOH aqueous solution.

Catalyst	$E_{1/2}$	Ref.
N-Co_2C HS/EC	**0.82** (V vs. RHE)	**This work**
Co_3C-GNRs	0.77 (V vs. RHE)	5
Co_3C-NB	0.748 (V vs. RHE)	6
Co_2C/rGO	-0.19 V (V vs. Ag/AgCl)	7
$Mn_{0.9}Fe_{2.1}C$/NC	0.78 (V vs. RHE)	8
MoCoZn/NCNTA	0.914 V (V vs. RHE)	9

$NeFe_3C$/ rGO40	0.80 (V vs. RHE)	[10]
Co/MoC@N-C	0.824 (V vs. RHE)	[11]
PB@ Met-700	0.853 (V vs. RHE)	[12]
NS-GR/Fe_3C	0.859 (V vs. RHE)	[13]
C@CoC_x	~ 0.8 (V vs. RHE)	[14]
Fe_3C/N@Co-doped CNF	0.8 V (V vs. RHE)	[15]
FeCo-WC/NC	0.85 (V vs. RHE)	[16]
Co@WC_{1-x}/NCNTs	0.81 (V vs. RHE)	[17]
$Co_6Mo_6C_2$-Co@NC	0.803 (V vs. RHE)	[18]

Table S3 Overpotential values at 10mA cm^{-2} of N-Co_2C HS/EC and the reported Co carbide catalysts for OER in 1 M KOH aqueous solution.

Catalyst	Overpotential (mV)	Ref.
N-Co_2C HS/EC	**278**	**This work**
Co_3C-NB	358	[6]
MoCoZn/NCNTA	445	[9]
Co/MoC@N-C	290	[11]
PB@Met-700	390	[12]
NS-GR/Fe_3C	397	[13]
Co@WC_{1-x}/NCNTs	330	[17]
$Co_6Mo_6C_2$-Co@NC	268	[18]

References

1. Z. Li, H. Yang, H. Sun, S. Liang, G. Lu, Z. Liu and S. Kou, *ACS Sustainable Chem. Eng.* , 2021, **9**, 4498-4508.
2. *MedeA® Materials Modeling Software Environment*, 2019, Materials Design, Inc.: San Diego, CA, USA.
3. J. P. Perdew, K. Burke and M. Ernzerhof, *Phys Rev Lett*, 1996, **77**, 3865-3868.
4. J. K. Nørskov, J. Rossmeisl, A. Logadottir, L. Lindqvist, J. R. Kitchin, T. Bligaard and H. Jónsson, *J. Phys. Chem. B*, 2004, **108**, 17886-17892.
5. X. Fan, Z. Peng, R. Ye, H. Zhou and X. Guo, *ACS Nano*, 2015, **9**, 7407-7418.

6. X. Ma, K. Li, X. Zhang, B. Wei, H. Yang, L. Liu, M. Zhang, X. Zhang and Y. Chen, *J. Mater. Chem. A*, 2019, **7**, 14904-14915.
7. M. D. Meganathan, S. Mao, T. Huang and G. Sun, *J. Mater. Chem. A*, 2017, **5**, 2972-2980.
8. C. Lin, X. Li, S. S. Shinde, D.-H. Kim, X. Song, H. Zhang and J.-H. Lee, *ACS Appl. Energy Mater.*, 2019, **2**, 1747.
9. Y. Wang, F. Yan, X. Ma, C. Zhu, X. Zhang and Y. Chen, *Electrochim. Acta*, 2021, **367**, 137522-137530.
10. H. Huang, Y. Chang, J. Jia, M. Jia and Z. Wen, *Int. J. Hydrogen Energy*, 2020, **45**, 28764-28773.
11. H. Huang, L. Kong, M. Liu, J. He, W. Shuang, Y. Xu and X.-H. Bu, *J. Energy Chem.* , 2021, **59**, 538-546.
12. Y. Lian, K. Shi, H. Yang, H. Sun, P. Qi, J. Ye, W. Wu, Z. Deng and Y. Peng, *Small*, 2020, **16**, 1907368.
13. K. Kohila Rani, C. Karuppiah, S. F. Wang, S. O. Alaswad, P. Sireesha, R. Devasenathipathy, R. Jose and C. C. Yang, *Ultrason. Sonochem.*, 2020, **66**, 105111-105119.
14. S. A. Rasaki, H. Shen, T. Thomas and M. Yang, *ACS Appl. Nano Mater.*, 2019, **2**, 3662-3670.
15. G.-H. An, Y.-G. Lee and H.-J. Ahn, *J. Alloys Compd.*, 2018, **746**, 177-184.
16. L. Xu, S. Wu, D. Deng, C. Wang, J. Qian, G. Lu and H. Li, *J. Alloys Compd.*, 2021, **868**, 159236-159242.
17. J. Cai, X. Zhang, M. Yang, Y. Shi, W. Liu and S. Lin, *J. Power Sources*, 2021, **485**, 229251-229260.
18. Y. Li, Z. Yin, M. Cui, S. Chen and T. Ma, *Mater. Today Energy*, 2020, **18**, 100565-100571.